Multiscale analysis of Klf10's impact on the passive mechanical properties of murine skeletal muscle

Y Tatarenko, M Li, P Pouletaut, M Kammoun, J R Hawse, V Joumaa, W Herzog, S Chatelin, Sabine F Bensamoun

Multiscale analysis of Klf10's impact on the passive mechanical properties of murine skeletal muscle

Y. Tatarenko[1,2], M. Li[3], P. Pouletaut[1], M. Kammoun[1], J.R. Hawse[4], V. Joumaa[3], W. Herzog[3], S. Chatelin[2], S. F. Bensamoun[1]

[1]Sorbonne University, Université de Technologie de Compiègne, CNRS UMR 7338, Biomechanics and Bioengineering, Compiègne, France

[2]ICube, CNRS UMR 7357, University of Strasbourg, Strasbourg, France

[3]University of Calgary, Faculty of Kinesiology, Human Performance Laboratory, Calgary, Alberta, Canada

[4]Department of Biochemistry and Molecular Biology, Mayo Clinic, Rochester, MN, USA

Corresponding author:

Sabine F. Bensamoun
Université de Technologie de Compiègne (UTC)
Laboratoire Biomécanique et Bioingénierie - UMR CNRS 7338
Rue Roger Couttolenc
CS 60319
60203 Compiègne cedex
France
Tel: (33) 03 44 23 43 90
E-mail address: sabine.bensamoun@utc.fr

HIGHLIGHTS

- Role of Klf10 on the passive behavior of muscle at three organizational scales.
- Klf10 impacts differentially the passive properties of the soleus and EDL muscles.
- Lack of Klf10 expression does not change the passive behavior of myofibrils.
- Disruption of Klf10 on skeletal muscle is primarily at the microscopic scale.

GRAPHICAL ABSTRACT

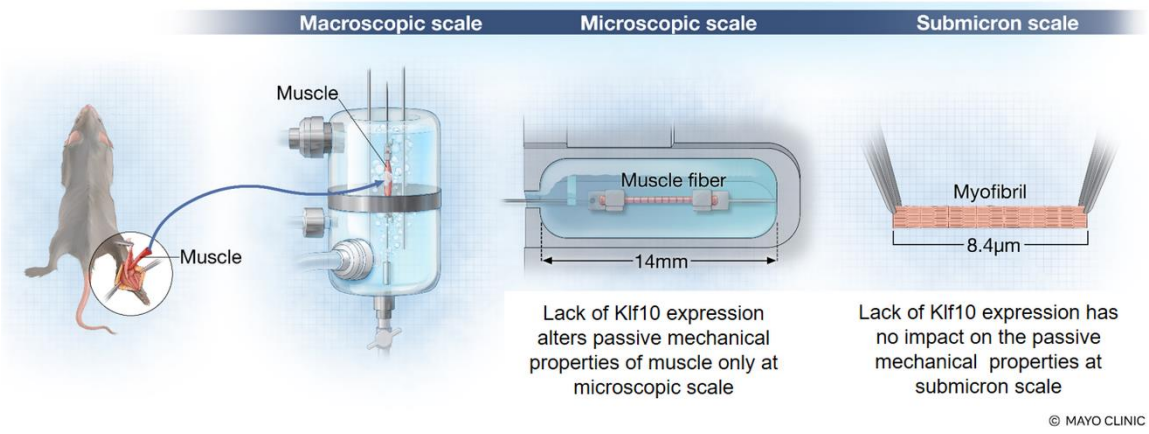

ABSTRACT

Skeletal muscle is a hierarchical structure composed of multiple organizational scales. A major challenge in the biomechanical evaluation of muscle relates to the difficulty in evaluating the experimental mechanical properties at the different organizational levels of the same tissue. Indeed, the ability to integrate mechanical properties evaluated at various levels will allow for improved assessment of the entire tissue, leading to a better understanding of how changes at each level evolve over time and/or impact tissue function, especially in the case of muscle diseases.

Therefore, the purpose of this study was to analyze a genetically engineered mouse model (Klf10 KO: Krüppel-Like Factor 10 knockout) with known skeletal muscle defects to compare the mechanical properties with wild-type (WT) controls at the three main muscle scales: the macroscopic (whole muscle), microscopic (fiber) and submicron (myofibril) levels. Passive mechanical tests (ramp, relaxation) were performed on two types of skeletal muscle (soleus and extensor digitorum longus (EDL)).

Results of the present study revealed muscle-type specific behaviors in both genotypes only at the microscopic scale. Interestingly, loss of Klf10 expression resulted in increased passive properties in the soleus but decreased passive properties in the EDL compared to WT controls. At the submicron scale, no changes were observed between WT and Klf10 KO myofibrils for either muscle; these results demonstrate that the passive property differences observed at the microscopic scale (fiber) are not caused by sarcomere intrinsic alterations but instead must originate outside the sarcomeres, likely in the collagen-based extracellular matrix. The macroscopic scale revealed similar passive mechanical properties between WT and Klf10 KO hindlimb muscles.

The present study has allowed for a better understanding of the role of Klf10 on the passive mechanical properties of skeletal muscle and has provided reference data to the literature which could be used by the community for muscle multiscale modeling.

Keywords: multiscale, mechanical properties, Klf10, mouse, skeletal muscle

1. Introduction

Striated skeletal muscle represents approximately 40 % of the human body mass that is multifunctional and highly adaptive to physiological and pathological conditions that may result in muscle hypertrophy (due to increased mechanical load) or atrophy (inactivity, chronic disease states) (Adams et al., 2003). From a structural point of view, striated skeletal muscle tissue is a complex, hierarchical system which can be classified into four primary scales (Tatarenko et al., 2022): macroscopic (mouse muscle diameter: about 1-3 cm), mesoscopic (mouse single fascicle diameter: about 0.5-30 mm), microscopic (mouse single muscle fiber diameter: 10-100 µm) and submicron (mouse single myofibril diameter: about 1-3 µm). The macroscopic scale is represented by the whole muscle and the different collagen sheaths. Both *in vivo* and *in vitro* techniques are currently used to characterize the morphological and mechanical properties of an entire skeletal muscle. The mesoscopic scale corresponds to the fascicles, which are surrounded by the perimysium tissue and is poorly characterized in the literature (Meyer and Lieber, 2011). The microscopic scale is defined by a single muscle fiber that is surrounded by the endomysium tissue, and *in vitro* mechanical techniques have been used to analyze its mechanical properties. Structural analysis and orientation of fibers within a muscle can be determined with specialized imaging techniques, such as diffusion tensor imaging (Correia et al., 2018), ultrasound (Ternifi et al., 2020) and multiphoton microscopy (Syverud et al., 2017). The submicroscopic scale is composed of myofibril filaments which can be mechanically assessed by only a few research groups around the world (Herzog et al., 2014; Linke et al., 2000).

There have been studies aimed at analyzing tissues at different structural levels. Brynnel et al. (2018) compared the passive properties between two fiber types (slow twitch and fast twitch) of muscles in mice. Moreover, for the same animal model (rabbit), Ward et al. (2020) compared the passive mechanical properties between fibers, bundles, fascicles and whole muscle. Meyer

et al. (2011) and Wood et al. (2014) compared the passive properties between fibers and bundles in mice, and Marcucci et al. (2019) compared the mechanical behavior between slow and fast fibers and bundles in humans. These models, based on experimental data, illustrated the importance of each scale on the global tissue response, and the difficulty in experimentally determining the mechanical properties at each scale of interest.

One of the major challenges in the biomechanical assessment of skeletal muscle relates to the current inability to integrate the mechanical properties at each primary scale and to evaluate changes of these properties over time to better understand the development and progression of muscle disorders and diseases. Indeed, some studies have demonstrated the impact of alterations in the structural and functional properties at different levels from the same tissue (tendon (Aghaei et al., 2021); myocardium (Tueni et al., 2022); soleus muscle (Bensamoun et al., 2006)). In addition, it has been demonstrated that genetic disorders resulting in muscle disease, such as Duchenne muscular dystrophy (Desguerre et al., 2012), have a strong effect on different structural scales leading to changes in whole muscle mechanical properties. A recent publication (Pouletaut et al., 2023) provided a better understanding of passive mechanical properties at the macro-micro and submicron scales, for healthy slow and fast twitch muscles. The results have demonstrated that the Young's modulus and passive stresses have higher values for the slow twitch (soleus) compared to the fast twitch (EDL: extensor digitorum longus) muscle at only the macroscopic scale. This study showed the relevance of the choice of the scale to study the impact of muscle type.

As a continuation of Pouletaut's study, a genetically modified mouse model, in which the Krüppel-like factor 10 (Klf10) gene was knocked-out, has been utilized in the present study, given that deletion of Klf10 is known to result in passive mechanical changes at the microscopic scale (*i.e.* slow and fast muscle fiber) (Kammoun et al., 2016; Kammoun et al., 2017). Thus, the purpose of this study was to analyze the passive mechanical properties at the macroscopic,

microscopic and submicron scales (Fig. 1), on mouse soleus and EDL muscles, to determine how the macroscopic mechanical behavior of muscle is impacted by the properties of its subcomponents at the microscopic and submicron scales in both healthy and Klf10 knockout muscle tissues.

2. Material and Methods

2.1. Animals

In agreement with our previous studies characterizing the role of Klf10 on the mechanical properties of adult female mouse skeletal muscle, we used 3-month-old WT (wild type) and KLF10 KO (knockout) female mice generated from heterozygous breeding. All mice were maintained in a temperature-controlled room (22 ± 2°C) with a light/dark cycle of 12 hours. Animals had free access to water and were fed a standard laboratory chow *ad libitum*. Anesthesia was performed via an isoflurane vaporizer (MiniHUB V2, TEM SEGA) device by inhalation from 3 $mg.L^{-1}$ to 1.5 $L.min^{-1}$ during muscle dissection. Following dissection, mice were euthanized by cervical dislocation according to the guidelines for the care and use of experimental animals. The protocol was approved by the French ministry of higher education, research, and innovation (Permit Number: DUO-4776) as well as the local ethics committee (CREMEAP; Permit Number: APAFIS #8905-2021011109249708).

2.2. Macroscopic scale

2.2.1. Preparation of the skeletal muscles and experimental set up

Soleus (N_{WT} = 9, N_{KO} = 6) and EDL (N_{WT} = 9, N_{KO} = 8) muscles were carefully harvested from the left hindlimb to ensure that muscles were not stretched during dissection and with confirmation that no residual tissue from surrounding muscles was carried forward. For muscle isolation, a suture (Sofsilk^{TM}, 4-0, 1.5Metric) was tied around the distal and proximal tendons; then tendons were cut and removed, and muscles were placed in a bath containing a

physiological solution (50 mL sodium bicarbonate, 10 mL calcium chloride dihydrate, 9.6 $g.L^{-1}$ Krebs-Henseleit buffer powder) maintained at a temperature of 25 °C, pH 7.3 and a constant oxygenation (95 % O2 and 5 % CO2) to mimic the *in vivo* environment (Fig. 1). Subsequently, the proximal and the distal parts of the muscle were connected to a dual mode force transducer (300C-LR dual-mode muscle lever, Aurora Scientific, Ontario, Canada) and to a hook, respectively. A pair of flat platinum electrodes, connected to an external stimulator set at 1 A, were placed on each side of the muscle. A SI610A Dynamics Muscle Control v5.420 software (Aurora Scientific, Ontario, Canada) was used to control the displacement of the lever arm to stretch the muscle at different velocities.

Prior to performing the passive mechanical tests, the muscle was placed at its optimal length (L_o), *i.e.* the length where the muscle developed its maximal isometric force. Optimal length was obtained for each muscle as follows. First, the muscle was set to its resting length (L_r), which corresponds to the length where muscle develops a stable force of 10 mN (Canon et al., 2008; Toscano et al., 2010), by applying three successive tetanus and three successive twitch contractions. Each stimulation was spaced 30 s apart and both impulses were performed at a 40 Hz frequency for a period of 0.7 s (tetanus test) and instantaneously (twitch test). Between each stimulation, a stretch was applied to the muscle to keep the initial force level of 10 mN constant. Once L_r had been determined in this manner, the optimal length (L_o) was obtained by applying successive twitch impulses, spaced 30 s apart, and by increasing the muscle length by increments of 0.25 mm between each twitch until the muscle reached its maximal isometric force.

2.2.2. Passive mechanical properties using ramp and relaxation tests

Preconditioning of the muscle samples was performed at L_o. Each sample underwent a stretch-release cycle, repeated two times spaced 5 min apart (Canon et al., 2008). The decrease of the hysteresis value was used to control the efficiency of the preconditioning.

After a rest of 5 min, soleus and EDL muscles underwent a ramp test with the stretch-release cycle consisting of a stretch of 25% of optimal length ($L_o \approx 10$ mm) at a slow velocity of 1.67% $L_o.s^{-1}$ (about 0.167 $mm.s^{-1}$) followed by a release at the same velocity, allowing for the measurement of the instantaneous force (F_{i_Ramp}) reached at the maximum of the stretch. The force-displacement curve was recorded, and a stress-strain curve was generated to measure the Young's modulus (E) in the linear part of the loading curve between 60 and 80% of the maximal strain (Hollenstein et al., 2006).

After a rest of 5 min, the viscoelastic properties were characterized through a relaxation test using a fast stretching velocity of 5 $L_o.s^{-1}$ (about 50 $mm.s^{-1}$) with an amplitude of stretch of 25% L_o. Three parameters were measured: 1) the dynamic force (F_d), corresponding to the maximum force reached at the end of the stretch, 2) the static force (F_{s_Relax}), corresponding to the steady state force reached at the end of the holding period (*i.e.* at 250 s), and 3) the half time of relaxation ($t_{1/2}$).

All forces (F_{s_Ramp}, F_d, F_{s_Relax}) were normalized relative to the initial cross-sectional (CSA) area of the respective muscle to determine the dynamic (σ_d), the instantaneous (σ_{i_Ramp}) and the static (σ_{s_Relax}) stresses. The cross-sectional area was calculated using the following equation (Del Prete et al., 2008):

$$CSA(mm^2) = \frac{m\ (mg)}{L_f(mm) * 1.06\ (mg\ .mm^{-3})} \quad (1)$$

where 1.06 ($mg.mm^{-3}$) is the density of mammalian skeletal muscle, (m) is the muscle mass and (L_f) the optimal fiber length which was calculated by multiplying the value L_o with the muscle

length ratio (0.44 for the EDL and 0.71 for soleus) as indicated in the literature (Del Prete et al., 2008).

Following completion of the passive testing, muscles were removed from the bath and weighed using an analytical laboratory balance (BP61S, SARTORIUS, Göttingen, Germany).

2.3. Microscopic scale

2.3.1. Preparation of muscle fibers and experimental set up

Skinned muscle fibers from an additional 5 WT and 5 KO mice were isolated from soleus (N_{WT} = 17, N_{KO} = 16) and EDL (N_{WT} = 16, N_{KO} = 15) muscles from the left hindlimb. Following disection, muscles were permeabilized at 4 °C in a skinning solution with successive added percentages of glycerol (12.5, 25 and 50 %) (Kammoun et al., 2016; Toursel et al., 2002; West et al., 2013). The muscle samples were then stored in 50% glycerol / 50% relaxing solution at -20 °C for a maximum of 5 weeks. Subsequently, using a light microscope (Leica™ M80, Wetzlar, Germany), muscle fibers were isolated and placed in a small bath (14 x 4 mm) (Fig. 1) filled with the relaxing solution, corresponding to the skinning solution, at a controlled temperature of 25 °C.

2.3.2. Passive mechanical tests performed with single muscle fibers

Single muscle fibers were attached at each extremity with an aluminium T-clip (Photofabrication, St Neots, UK) respectively connected to a force transducer (5 mN) and to a motor (1400A - 802D Permeabilized Fiber Test Apparatus - Aurora Scientific). Immediately prior to mechanical testing, each fiber was manually stretched to a sarcomere length of 2.4 µm by the same operator. The control of this length was performed with the placement of a region of interest over 3 sarcomeres using ASI 900B video sarcomere length tools (Aurora Scientific, Aurora, Ontario, Canada). After, its slack length ($L_s \approx 2$ mm) was measured using an optical microscope (Leica™ DM IL LED, Wetzlar, Germany), composed of a 10 mm graticule in the eyepiece, at a magnification of 20X. The average fiber diameter was determined using several

measurements along the fiber length. Subsequently, each fiber underwent two preconditioning tests followed by two passive mechanical tests (ramp stretch, stress-relaxation) as previously described (Kammoun et al., 2016).

Preconditioning tests were performed to limit the impact of the viscous effect on the myofibrils (Rehorn et al., 2014). Accordingly, each fiber was stretched to 150% L_s (about 3 mm) at velocity of 0.00167 $L_s.s^{-1}$ (about 0.00333 mm s^{-1}) and relaxed at the same velocity. After a 5 min rest period at the slack length, this preconditioning test was repeated twice. The hysteresis loop was plotted for each preconditioning run. The hysteresis area was calculated and the decrease in the hysteresis value was used to control the efficiency of preconditioning (Kammoun et al., 2016).

The first passive mechanical test was a ramp stretch. The fibers were stretched to 150 % L_s (about 3 mm) with a velocity of 0.033 $L_s.s^{-1}$ (about 0.066 mm s^{-1}) and released at the same velocity, allowing the measurement of the instantaneous force (F_{i_Ramp}) reached at the end of the stretch. As with the whole muscle test, the Young's modulus (E) was calculated using an identical method (Hollenstein et al., 2006).

The second passive mechanical test was a relaxation test. Over a period of 60 s, the fiber was rapidly stretched to 150 % L_s (about 3 mm) at a high velocity of 3.3 $L_s.s^{-1}$ (about 6.6 mm s^{-1}) and released to its slack length. The dynamic force F_d, corresponding to the maximal force value, reached at the end of the stretch, and the static force F_{s_Relax} measured at the end of the test, before the fiber was released, were recorded. In addition, the half time of relaxation was measured.

All measured forces (F_{i_Ramp}, F_d, F_{s_Relax}) were divided by the initial average anatomical cross-sectional area of the fiber to obtain dynamic (σ_d), instantaneous (σ_{i_Ramp}) and static (σ_{s_Relax}) stresses.

2.4. Submicron scale

2.4.1. Preparation of the myofibrils and experimental set up

Myofibrils were extracted from the soleus (N_{WT} = 11, N_{KO} = 11) and EDL (N_{WT} = 11, N_{KO} = 11) muscles of an additional 6 WT and 6 KO mice. To isolate the myofibrils, muscles were first skinned as described above. A small piece of the skinned muscles (about 5 mm in length and 2 mm in width) was placed in a microcentrifuge tube containing rigor solution and vortexed to separate individual myofibrils (Joumaa et al., 2008).

2.4.2. Passive mechanical test performed with myofibrils

Myofibrils were placed in a bath on the stage of an inverted microscope and attached to a glass needle at one end, and to a nanolever at the other end (Fig. 1), allowing for length changes and force measurements, respectively (Powers et al., 2017). The sarcomere striation pattern of the myofibrils was projected onto a linear photodiode array for determination of individual sarcomere lengths. The diameter of the myofibrils was measured at a magnification of 250X and used to determine the cross-sectional area of myofibrils.

Subsequently, myofibrils were set at an average sarcomere length of 2.4 µm. They were then passively stretched at a speed of 0.1 µm.s^{-1} to an average sarcomere length of 3.4 µm. The stretch was held for 20 seconds until a steady-state force was reached, and then released. Passive force reached at steady-state, *i.e* at the end of the test, was determined and converted to static stress (σ_s) by dividing the recorded force by the cross-sectional area of each myofibril.

2.5. Statistical analysis

The SystatTM V11 software (Systat Software Inc., CA, USA) was used for all statistical analyses. Non-parametric two-sample Mann-Whitney tests were used to compare all parameter

values at a given scale between the WT and KLF10 KO genotypes. Results were considered significant for $p < 0.05$.

3. Results

3.1. Comparison between Klf10 KO and WT soleus across scales

Figure 2 depicts the comparison of the stress curves between WT and Klf10 KO soleus at each scale.

At the macroscopic scale (Fig. 3), all passive parameters (σ_{i_Ramp}, E, σ_d, σ_{s_Relax}, $t_{1/2}$) obtained for WT controls and Klf10 KO soleus muscle were within the same range (Fig. 3A, Table 1A). However, none of these reached statistical significance (Table 2).

At the microscopic scale, a significant difference ($P < 0.01$) was observed for all of the parameters analyzed (Fig. 3B, Table 1B, Table 2), excepted for the half relaxation time, between fibers extracted as a function of mouse genotype.

At the submicron scale, no significant difference was found for the static stresses (σ_s) of myofibril filament between WT and Klf10 KO animals (Fig. 3C, Table 1C, Table 2). Of note, there was much more variability between individual myofibrils isolated from Klf10 KO mice.

To conclude, particularly at the microscopic scale, there were significantly higher values ($P < 0.01$) in the passive stresses and Young's modulus of the Klf10 KO soleus fibers.

3.2. Comparison between Klf10 KO and WT EDL across scales

Figure 4 depicts the comparison of the stress curves between WT and Klf10 KO EDL at each scale.

At the macroscopic scale (Fig. 5A), all passive parameters (σ_{i_Ramp}, E, σ_d, σ_{s_Relax}) for the Klf10 KO were slightly higher compared to the WT control (Table 3A). However, none of these, including the half relaxation time, reached statistical significance (Table 4).

At the microscopic scale (Fig. 5B), a significant difference ($P < 0.01$) was observed for all of the parameters analyzed (Table 3B, Table 4), excepted for the half relaxation time, between WT and Klf10 KO fibers.

At the submicron scale, no significant difference was found for the static stresses (σ_s) of myofibril filaments between WT and Klf10 KO animals (Fig. 5C, Table 3C, Table 4).

Overall, particularly at the microscopic scale, there were significant lower values ($P < 0.01$) in the passive stresses and Young's modulus of the EDL muscle in the absence of Klf10 expression.

4. Discussion

Klf10 is known to be highly expressed in skeletal muscle (Subramaniam et al., 1995; Subramaniam et al., 1998), and we have previously reported multiple scale impacts through phenotypic differences in the skeletal muscle organization: increase of fiber diameter (Kammoun et al., 2017), shorter sarcomere length (Kammoun et al., 2020), etc. We have also discovered substantial differences in mitochondrial localization and function (Kammoun et al., 2020), particularly in the soleus muscle. At the molecular level, we have also demonstrated significant impacts of Klf10 on muscle metabolism (Baroukh et al., 2022).

The basis for the present study was to analyze the impact of Klf10 gene deletion on the passive mechanical properties of fast and slow twitch skeletal muscles at the macroscopic, microscopic and submicron scales. More specifically, at each scale, we have evaluated only the linear elastic properties of this tissue and have compared the results to those obtained from WT

littermate controls. Future directions of this work will be to apply different strain rates to the muscle tissue, with passive mechanical tests, which would allow for the study of the non-linear responses such as Meyer's study (Meyer et al., 2011b). In addition, it is of interest to use the same amplitude of strain for all specimens in order to compare the mechanical behaviors between the scales.

An efficient way to describe the mechanical behaviors of a muscle at different scales is through finite element modeling (Wheatley et al., 2016; Wheatley et al., 2017). Such modeling includes a constitutive law with multiscale parameters (mechanical behavior of the underlying components, microscopic and macroscopic architecture, fast and slow fibers, *etc.*) by homogenization methods (May-Newman et al., 1998; Röhrle et al., 2012, Spyrou et al., 2017, 2019). The macroscopic behavior of the tissue is predicted by complex scale shifting operations representing the intersecting phenomena between the components. In spite of these different elements, the multiscale link between mechanical properties of muscle fibers and the global homogenized functional behavior of striated skeletal muscle remains underexplored. One of the reasons for this state of affairs is that the development and validation of such muscle models requires not only the measurement of experimental data of anatomical and morphological types, but also functional (or mechanical) data at both the macroscopic, microscopic and submicron scales.

To begin to address this void, we sought to evaluate the biomechanical properties of skeletal muscle at various scales and to explore how such mechanical evaluation may reveal known structural phenomena. Results from the present study indicate that only the passive mechanical behaviors at the microscopic scale were significantly different between Klf10 KO and WT animals for both of the muscles analyzed (soleus and EDL). It should be noted that opposite variations in the passive mechanical parameters for soleus and EDL were observed whereby the KO fibers showed higher and lower values compared to WT fibers, respectively. These

results demonstrated that Klf10 has a fiber-type specific impact on skeletal muscle at the microscopic scale. This may be due to the different roles of Klf10 on the oxidative and glycolytic signaling pathways (Kammoun et al., 2017; Kammoun et al., 2020).

To gain insight into the origin of the Klf10 KO passive behaviors observed at the different scales, myofibril filaments were tested as they represent the primary mechanical properties of the sarcomere without the confounding effect of any extra-cellular passive components. Interestingly, similar values were found between WT and Klf10 KO myofibrils for both muscles. Since the primary, and virtually exclusive, passive forces in myofibrils originate from the sarcomeric protein titin, it is safe to assume that the titin isoforms in Klf10 KO and WT are similar and have similar mechanical properties. Indeed, a complementary analysis (Pouletaut et al., 2021) on the molecular weights of titin for WT and Klf10 KO mice showed that there is no difference in titin isoforms. Therefore, it may reasonably be concluded that the changes in the passive properties found at the fiber level do not originate from sarcomeric structures. Thus, the observed fiber-type specific changes in passive force in Klf10 KO mice are likely in the collagen-based extracellular matrix surrounding the fiber.

Of future interest is to additionally incorporate characterization at the mesoscopic scale (*i.e.* the fascicle), but at present established and validated techniques have not been reported (Meyer et al., 2011a). Fascicles are surrounded by the perimysium and are composed of fibers also surrounded with collagenous extracellular tissues (endomysium). Therefore, it is likely that the extracellular matrix contributes to the overall mechanical properties of the whole muscle. Indeed, Brashear et al. (2021) showed that the structural organization of the collagen fibers within the ECM impacts the mechanical properties of the tissue. Interestingly, we have previously demonstrated that loss of Klf10 expression results in a modification of the collagen network which may also contribute to altered mechanical properties (Doucet et al., 2011; Gumez et al., 2010). In addition, DiMario et al. (2018) demonstrated an impact of Klf10 in the

fibrosis process of the Duchenne myopathy disease. However, similar passive mechanical properties were observed between WT and Klf10 KO hindlimb muscles in the present study. It is possible that use of higher strains in these tests would allow for the detection of macroscopic differences that are not observed with lesser strains. In addition, it is of interest to analyze the role of Klf10 in mediating the composition and maintenance of extracellular matrix components such as collagens in soleus and EDL muscles. Moreover, the cytoskeleton and/or cytoplasm components and properties of muscle fiber cells could also be analyzed.

Recently, non-invasive imaging techniques such as elastography (Kammoun et al., 2019; Qin et al., 2013) make it possible to characterize such mechanical properties *in vivo* allowing for longitudinal assessment and ultimately non-invasive monitoring of pathological progression in the case of specific muscle diseases. In a previous study (Ternifi et al., 2020), ultrasound shear wave (SWE) elastography was performed on Klf10 KO mice and the passive mechanical behaviors of a group of muscles were measured as it was not possible to independently analyze slow and fast twitch muscles. Nevertheless, non-invasive imaging techniques are promising tools for assessment of selected mechanical properties at the macroscopic scale, but at present, *in vitro* multiscale investigation is still required for comprehensive analysis of the mechanical properties at the different structural levels of muscle.

It has been shown that bones and tendons adapt their mechanical properties when muscles change their function, for example in disease, aging or disuse. Such adaptations also take place within the different structural levels of muscle, as reflected in the data presented here, thus, possibly providing a better understanding of the effects of Klf10 and the mechanisms by which such adaptations are initiated. This knowledge may serve in multiscale finite element models of muscles in general and Klf10 KO muscles specifically. Our results regarding the differential impact of Klf10 at the different structural levels may be useful in the modeling of other genetic muscle diseases (such as Duchenne myopathy (DiMario et al., 2018)) when trying to identify

mechanisms of action, treatment therapies, and the prediction of function through disease-specific muscle models.

Acknowledgements

This work was supported by Idex Sorbonne University SU-19-3-EMRG-12 (S.F.B), the Research Department of UTC within the framework of AMI International (S.F.B) and the National Institutes of Health (USA), Grant No. R01 DE14036 (J.R.H.). This work was also supported by the Interdisciplinary Thematic Institute ITI HealthTech, as part of the ITI 2021-2028 program of the University of Strasbourg, CNRS and Inserm, through IdEx Unistra (ANR-10-IDEX-0002) (S.C) and SFRI (STRAT'US project, ANR-20-SFRI-0012 (S.C). We would also like to thank Frank Corl of the Mayo Clinic for the artistic rendering provided in Fig. 1.

Declaration of competing interest

The authors declare that they have no competing financial interests or personal relationships that could have appeared to influence the work reported in this paper.

References

Adams, G.R., Caiozzo, V.J., Baldwin, K.M., 2003. Skeletal muscle unweighting: spaceflight and ground-based models. Journal of Applied Physiology 95, 2185–2201. https://doi.org/10.1152/japplphysiol.00346.2003

Aghaei, A., Bochud, N., Rosi, G., Naili, S., 2021. Wave propagation across a functionally graded interphase between soft and hard solids: Insight from a dynamic surface elasticity model. Journal of the Mechanics and Physics of Solids 151, 104380. https://doi.org/10.1016/j.jmps.2021.104380

Baroukh, N., Canteleux, N., Lefèvre, A., Dupuy, C., Martias, C., Presset, A., ... & Nadal-Desbarats, L. (2022). Serum and soleus metabolomics signature of Klf10 knockout mice to identify potential biomarkers. Metabolites, 12(6), 556. https://doi.org/10.3390/metabo12060556

Bensamoun, S., Stevens, L., Fleury, M.J., Bellon, G., Goubel, F., Ho Ba Tho, M.C., 2006. Macroscopic–microscopic characterization of the passive mechanical properties in rat soleus muscle. Journal of Biomechanics 39, 568–578. https://doi.org/10.1016/j.jbiomech.2004.04.036

Brashear, S. E., Wohlgemuth, R. P., Gonzalez, G., & Smith, L. R., 2021. Passive stiffness of

fibrotic skeletal muscle in mdx mice relates to collagen architecture. The Journal of physiology, 599(3), 943-962. https://doi-org.ezproxy.utc.fr/10.1113/JP280656
Brynnel, A., Hernandez, Y., Kiss, B., Lindqvist, J., Adler, M., Kolb, J., ... & Granzier, H. L. (2018). Downsizing the molecular spring of the giant protein titin reveals that skeletal muscle titin determines passive stiffness and drives longitudinal hypertrophy. Elife, 7, e40532. https://doi.org/10.7554/eLife.40532
Canato, M., Dal Maschio, M., Sbrana, F., Raiteri, R., Reggiani, C., Vassanelli, S., Megighian, A., 2010. Mechanical and Electrophysiological Properties of the Sarcolemma of Muscle Fibers in Two Murine Models of Muscle Dystrophy: Col6a1 and Mdx. Journal of Biomedicine and Biotechnology 2010, e981945. https://doi.org/10.1155/2010/981945
Canon, F., Gamet, D., Perot, C., 2008. Passive stiffness of rat soleus muscle from weaning to senescence. Computer Methods in Biomechanics and Biomedical Engineering 11, 49–50. https://doi.org/10.1080/10255840802296756
Correia, M., Deffieux, T., Chatelin, S., Provost, J., Tanter, M., Pernot, M., 2018. 3D elastic tensor imaging in weakly transversely isotropic soft tissues. Phys Med Biol 63, 155005. https://doi.org/10.1088/1361-6560/aacfaf
Desguerre, I., Arnold, L., Vignaud, A., Cuvellier, S., Yacoub-youssef, H., Gherardi, R. K., ... & Chazaud, B., 2012. A new model of experimental fibrosis in hindlimb skeletal muscle of adult mdx mouse mimicking muscular dystrophy. Muscle & nerve, 45(6), 803-814. https://doi.org/10.1002/mus.23341
Del Prete, Z., Musarò, A., Rizzuto, E., 2008. Measuring Mechanical Properties, Including Isotonic Fatigue, of Fast and Slow MLC/mIgf-1 Transgenic Skeletal Muscle. Ann Biomed Eng 36, 1281–1290. https://doi.org/10.1007/s10439-008-9496-x
DiMario, J. X. (2018). KLF10 gene expression modulates fibrosis in dystrophic skeletal muscle. The American journal of pathology, 188(5), 1263-1275. https://doi.org/10.1016/j.ajpath.2018.01.014
Doucet, J., Briki, F., Gourrier, A., Pichon, C., Gumez, L., Bensamoun, S., Sadoc, J.-F., 2011. Modeling the lateral organization of collagen molecules in fibrils using the paracrystal concept. J Struct Biol 173, 197–201. https://doi.org/10.1016/j.jsb.2010.11.018
Gumez, L., Bensamoun, S.F., Doucet, J., Haddad, O., Hawse, J.R., Subramaniam, M., Spelsberg, T.C., Pichon, C., 2010. Molecular structure of tail tendon fibers in TIEG1 knockout mice using synchrotron diffraction technology. J Appl Physiol (1985) 108, 1706–1710. https://doi.org/10.1152/japplphysiol.00356.2010Herzog, W., 2014. The role of titin in eccentric muscle contraction. Journal of Experimental Biology 217, 2825–2833. https://doi.org/10.1242/jeb.099127
Hollenstein, M., Nava, A., Valtorta, D., Snedeker, J.G., Mazza, E., 2006. Mechanical Characterization of the Liver Capsule and Parenchyma, in: Harders, M., Székely, G. (Eds.), Biomedical Simulation, Lecture Notes in Computer Science. Springer, Berlin, Heidelberg, pp. 150–158. https://doi.org/10.1007/11790273_17
Joumaa, V., Rassier, D.E., Leonard, T.R., Herzog, W., 2008. The origin of passive force enhancement in skeletal muscle. American Journal of Physiology-Cell Physiology 294, C74–C78. https://doi.org/10.1152/ajpcell.00218.2007
Kammoun, M., Pouletaut, P., Canon, F., Subramaniam, M., Hawse, J.R., Vayssade, M., Bensamoun, S.F., 2016. Impact of TIEG1 Deletion on the Passive Mechanical Properties of Fast and Slow Twitch Skeletal Muscles in Female Mice. PLOS ONE 11, e0164566. https://doi.org/10.1371/journal.pone.0164566
Kammoun, M., Même, S., Même, W., Subramaniam, M., Hawse, J.R., Canon, F., Bensamoun, S.F., 2017. Impact of TIEG1 on the structural properties of fast and slow twitch skeletal muscle. Muscle Nerve 55(3), 410-416. https://doi.org/10.1002/mus.25252
Kammoun, M., Ternifi, R., Dupres, V., Pouletaut, P., Même, S., Même, W., Szeremeta, F.,

Landoulsi, J., Constans, J.-M., Lafont, F., Subramaniam, M., Hawse, J.R., Bensamoun, S.F., 2019. Development of a novel multiphysical approach for the characterization of mechanical properties of musculotendinous tissues. Sci Rep 9, 7733. https://doi.org/10.1038/s41598-019-44053-1

Kammoun, M., Piquereau, J., Nadal-Desbarats, L., Même, S., Beuvin, M., Bonne, G., ... & Bensamoun, S. F. (2020). Novel role of Tieg1 in muscle metabolism and mitochondrial oxidative capacities. Acta Physiologica, 228(3), e13394. https://doi.org/10.1111/apha.13394

Kammoun, M., Pouletaut, P., Morandat, S., Subramaniam, M., Hawse, J.R., Bensamoun, S.F.. 2021. Krüppel-like factor 10 regulates the contractile properties of skeletal muscle fibers in mice. Muscle & Nerve 64(6), 765-769. https://dx.doi.org/10.1002/MUS.27412

Linke, W.A., 2000. Stretching molecular springs: elasticity of titin filaments in vertebrate striated muscle. Histol Histopathol 15, 799–811. https://doi.org/10.14670/HH-15.799

Marcucci, L., Bondì, M., Randazzo, G., Reggiani, C., Natali, A. N., & Pavan, P. G. (2019). Fibre and extracellular matrix contributions to passive forces in human skeletal muscles: An experimental based constitutive law for numerical modelling of the passive element in the classical Hill-type three element model. PLoS One, 14(11), e0224232. https://doi.org/10.1371/journal.pone.0224232

May-Newman, K., McCulloch, A.D., 1998. Homogenization modeling for the mechanics of perfused myocardium. Prog Biophys Mol Biol 69, 463–481. https://doi.org/10.1016/s0079-6107(98)00020-0

Meyer, G.A., Lieber, R.L., 2011a. Elucidation of extracellular matrix mechanics from muscle fibers and fiber bundles. Journal of Biomechanics 44, 771–773. https://doi.org/10.1016/j.jbiomech.2010.10.044

Meyer, G.A., McCulloch, A.D., Lieber, R.L., 2011b. A nonlinear model of passive muscle viscosity. Journal of biomechanical engineering 133(9):091007. https://doi.org/10.1115/1.4004993

Nierenberger, M., Rémond, Y., Ahzi, S., 2013. A new multiscale model for the mechanical behavior of vein walls. Journal of the Mechanical Behavior of Biomedical Materials 23, 32–43. https://doi.org/10.1016/j.jmbbm.2013.04.001

Pouletaut, P., Tatarenko, Y., Li, M., Joumaa, V.. Hawse, J.R., Herzog, W., Chatelin, S., Bensamoun, S.F., 2023. Multiscale mechanical characterization of rodent skeletal muscle. Journal of Biomechanics, *in press*. https://doi.org/10.1016/j.irbm.2023.100800

Powers, K., Joumaa, V., Jinha, A., Moo, E.K., Smith, I.C., Nishikawa, K., Herzog, W., 2017. Titin force enhancement following active stretch of skinned skeletal muscle fibres. Journal of Experimental Biology 220, 3110–3118. https://doi.org/10.1242/jeb.153502

Qin, E.C., Sinkus, R., Geng, G., Cheng, S., Green, M., Rae, C.D., Bilston, L.E., 2013. Combining MR elastography and diffusion tensor imaging for the assessment of anisotropic mechanical properties: a phantom study. J Magn Reson Imaging 37, 217–226. https://doi.org/10.1002/jmri.23797

Rehorn, M.R., Schroer, A.K., Blemker, S.S., 2014. The passive properties of muscle fibers are velocity dependent. Journal of Biomechanics 47, 687–693. https://doi.org/10.1016/j.jbiomech.2013.11.044

Röhrle, O., Davidson, J.B., Pullan, A.J., 2012. A physiologically based, multi-scale model of skeletal muscle structure and function. Front Physiol 3, 358. https://doi.org/10.3389/fphys.2012.00358

Subramaniam, M., Harris, S. A., Oursler, M. J., Rasmussen, K., Riggs, B. L., & Spelsberg, T. C. (1995). Identification of a novel TGF-β-regulated gene encoding a putative zinc finger protein in human osteoblasts. Nucleic acids research, 23(23), 4907-4912. https://doi.org/10.1093/nar/23.23.4907

Subramaniam, M., Hefferan, T. E., Tau, K., Peus, D., Pittelkow, M., Jalal, S., ... & Spelsberg, T. C. (1998). Tissue, cell type, and breast cancer stage-specific expression of a TGF-β inducible early transcription factor gene. Journal of cellular biochemistry, 68(2), 226-236. https://doi-org.ezproxy.utc.fr/10.1002/(SICI)1097-4644(19980201)68:2%3C226::AID-JCB9%3E3.0.CO;2-X

Spyrou, L.A., Agoras, M., Danas, K., 2017. A homogenization model of the Voigt type for skeletal muscle. Journal of Theoretical Biology 414, 50–61. https://doi.org/10.1016/j.jtbi.2016.11.018

Spyrou, L.A., Brisard, S., Danas, K., 2019. Multiscale modeling of skeletal muscle tissues based on analytical and numerical homogenization. Journal of the Mechanical Behavior of Biomedical Materials 92, 97–117. https://doi.org/10.1016/j.jmbbm.2018.12.030

Syverud, B.C., Mycek, M.A., Larkin, L.M., 2017. Quantitative, Label-Free Evaluation of Tissue-Engineered Skeletal Muscle Through Multiphoton Microscopy. Tissue Eng Part C Methods 23(10):616-626. https://doi.org/10.1089/ten.tec.2017.0284.

Tatarenko, Y., Pouletaut, P., Chatelin, S., F. Bensamoun, S., 2022. Passive and active mechanical tests at different scales of the skeletal muscle: a literature review. State of the Art in Bioengineering 2.

Ternifi, R., Kammoun, M., Pouletaut, P., Subramaniam, M., Hawse, J.R., Bensamoun, S.F., 2020. Ultrasound image processing to estimate the structural and functional properties of mouse skeletal muscle. Biomedical Signal Processing and Control 56, 101735. https://doi.org/10.1016/j.bspc.2019.101735

Toscano, A.E., Ferraz, K.M., de Castro, R.M., Canon, F., 2010. Passive stiffness of rat skeletal muscle undernourished during fetal development. Clinics 65, 1363–1369. https://doi.org/10.1590/S1807-59322010001200022

Toursel, T., Stevens, L., Granzier, H., Mounier, Y., 2002. Passive tension of rat skeletal soleus muscle fibers: effects of unloading conditions. J Appl Physiol (1985) 92, 1465–1472. https://doi.org/10.1152/japplphysiol.00621.2001

Tueni, N., Allain, J.-M., Genet, M., 2022. On the structural origin of the anisotropy in the myocardium: Multiscale modeling and analysis. https://hal.archives-ouvertes.fr/hal-03604234

Ward, S. R., Winters, T. M., O'Connor, S. M., & Lieber, R. L. (2020). Non-linear scaling of passive mechanical properties in fibers, bundles, fascicles and whole rabbit muscles. Frontiers in Physiology, 11, 211. https://doi.org/10.3389/fphys.2020.00211

West, T.G., Toepfer, C.N., Woledge, R.C., Curtin, N.A., Rowlerson, A., Kalakoutis, M., Hudson, P., Wilson, A.M., 2013. Power output of skinned skeletal muscle fibres from the cheetah (Acinonyx jubatus). Journal of Experimental Biology 216, 2974–2982. https://doi.org/10.1242/jeb.083667

Wheatley, B.B., Morrow, D.A., Odegard, G.M., Kaufman, K.R., Haut Donahue, T.L., 2016. Skeletal muscle tensile strain dependence: Hyperviscoelastic nonlinearity. Journal of the Mechanical Behavior of Biomedical Materials 53, 445–454. https://doi.org/10.1016/j.jmbbm.2015.08.041

Wheatley, B.B., 2017. Finite element analysis of skeletal muscle: a validated approach to modeling muscle force and intramuscular pressure (Doctoral dissertation). Colorado State University. http://hdl.handle.net/10217/181381

Wood, L. K., Kayupov, E., Gumucio, J. P., Mendias, C. L., Claflin, D. R., & Brooks, S. V. (2014). Intrinsic stiffness of extracellular matrix increases with age in skeletal muscles of mice. Journal of applied physiology, 117(4), 363-369. https://doi.org/10.1152/japplphysiol.00256.2014

Figure Legends

Fig. 1. Representation of the mechanical tests realized on healthy mouse at the macroscopic (muscle), microscopic (fiber) and submicron (myofibril) scales.

Fig. 2. Representative stress vs time curves for an exemplar ramp test (left side) and an exemplar relaxation test (middle side with a zoom of the initial stress on the right side), at the macroscopic (A), microscopic (B) and submicron (C) scales from wild type (WT) and Klf10 knockout (KO) soleus muscles. For the ramp test, the velocities were approximately 0.167 $mm.s^{-1}$, 66 $\mu m.s^{-1}$, 0.1 $\mu m.s^{-1}$ for muscle, fiber and myofibril, respectively. For the relaxation test, the velocities were approximately 50 $mm.s^{-1}$ and 6.6 $mm.s^{-1}$ for muscle and fiber, respectively.

Fig. 3. Boxplots of instantaneous stress (σ_{i_Ramp}), static stress (σ_s, σ_{s_Relax}), dynamic stress (σ_d), Young's modulus (E) and half relaxation time ($t_{1/2}$) values of the soleus muscle components at the (A) macro and (B) micro scales, and for the ramp test and the relaxation test. ** : $p < 0.01$ (Mann-Whitney's test).

Fig. 4. Representative stress vs time curves for an exemplar ramp test (left side) and an exemplar relaxation test (middle side with a zoom of the initial stress on the right side), at the macroscopic (A), microscopic (B) and submicron (C) scales from wild type (WT) and Klf10 knockout extensor digitorum longus (EDL) muscles. For the ramp test, the velocities were approximately 0.167 $mm.s^{-1}$, 66 $\mu m.s^{-1}$, 0.1 $\mu m.s^{-1}$ for muscle, fiber and myofibril, respectively. For the relaxation test, the velocities were approximately 50 $mm.s^{-1}$ and 6.6 $mm.s^{-1}$ for muscle and fiber, respectively.

Fig. 5. Boxplots of instantaneous stress (σ_{i_Ramp}), static stress (σ_s, σ_{s_Relax}), dynamic stress (σ_d), Young's modulus (E) and half relaxation time ($t_{1/2}$) values of the extensor digitorum longus (EDL) muscle components at the (A) macro and (B) micro scales, and for the ramp test and the relaxation test. * : $p < 0.05$; ** : $p < 0.01$ (Mann-Whitney's test).

Table 1

For the (A) macroscopic, (B) microscopic and (C) submicron scales, instantaneous stress (σ_{i_Ramp}), static stress (σ_s, σ_{s_Relax}), dynamic stress (σ_d), Young's modulus (E) and half relaxation time ($t_{1/2}$) values (mean ± sem) of the soleus muscle components for wild-type (WT) and knockout (KO) mice obtained with the ramp and relaxation tests. ** : $p < 0.01$ (Mann-Whitney's test).

(A) Macroscopic scale

	σ_{i_Ramp} (kPa)	E (kPa)	σ_{s_Relax} (kPa)	σ_d (kPa)	$t_{1/2}$ (ms)
WT (n = 8)	256.8 ± 8.1	1.52 ± 0.06	146.8 ± 4.2	368.3 ± 10.5	104.6 ± 4.0
KO (n = 9)	249.7 ± 14.7	1.52 ± 0.10	140.0 ± 7.3	361.0 ± 19.1	97.1 ± 3.0

(B) Microscopic scale

	σ_{i_Ramp} (kPa)	E (kPa)	σ_{s_Relax} (kPa)	σ_d (kPa)	$t_{1/2}$ (ms)
WT (n = 17)	212.6 ± 20.4	0.60 ± 0.06	108.9 ± 11.0	305.6 ± 26.1	64.9 ± 2.2
KO (n = 16)	321.3 ± 28.0**	0.97 ± 0.10**	174.4 ± 15.7**	444.7 ± 40.2**	68.4 ± 2.4

(C) Submicron scale

	σ_s (kPa)
WT (n = 11)	51.8 ± 6.4
KO (n = 11)	47.8 ± 7.7

Table 2

For the macroscopic, microscopic and submicron scales, p-value of Mann-Whitney test for the comparison, between wild-type (WT) and knockout (KO) soleus muscle components of the instantaneous stress (σ_{i_Ramp}), static stress (σ_{s_Relax}), dynamic stress (σ_d), Young's modulus (E) and half relaxation time ($t_{1/2}$) values (mean ± sem) obtained with the ramp and relaxation tests. ** : $p < 0.01$ (Mann-Whitney's test).

	σ_{i_Ramp}	E	σ_{s_Relax}	σ_d	$t_{1/2}$
Macroscopic scale (WT vs KO)	0.773	0.847	0.700	1.000	0.200
Microscopic scale (WT vs KO)	0.008	0.004	0.002	0.009	0.364

	σ_s
Submicron scale (WT vs KO)	0.526

Table 3

For the (A) macroscopic, (B) microscopic and (C) submicron scales, instantaneous stress (σ_{i_Ramp}), static stress (σ_s, σ_{s_Relax}), dynamic stress (σ_d), Young's modulus (E) and half relaxation time ($t_{1/2}$) values (mean ± sem) of the extensor digitorum longus (EDL) muscle components for wild-type (WT) and knockout (KO) mice obtained with the ramp and relaxation tests. ** : $p < 0.01$ (Mann-Whitney's test).

(A) Macroscopic scale

	σ_{i_Ramp} (kPa)	E (kPa)	σ_{s_Relax} (kPa)	σ_d (kPa)	$t_{1/2}$ (ms)
WT (n = 8)	193.1 ± 14.7	1.16 ± 0.10	110.3 ± 7.0	295.4 ± 18.2	98.4 ± 4.4
KO (n = 10)	171.0 ± 13.9	1.01 ± 0.08	96.7 ± 7.3	269.2 ± 17.2	108.6 ± 4.8

(B) Microscopic scale

	σ_{i_Ramp} (kPa)	E (kPa)	σ_{s_Relax} (kPa)	σ_d (kPa)	$t_{1/2}$ (ms)
WT (n = 16)	286.7 ± 34.0	0.86 ± 0.13	. 147.8 ± 19.9	396.9 ± 47.1	74.2 ± 7.6
KO (n = 15)	154.3 ± 10.8**	0.45 ± 0.04**	81.2 ± 5.8**	219.0 ± 15.4**	73.8 ± 5.4

(C) Submicron scale

	σ_s (kPa)
WT (n = 11)	42.5 ± 4.7
KO (n = 11)	41.6 ± 7.2

Table 4

For the macroscopic, microscopic and submicron scales, p-value of Mann-Whitney test for the comparison, between wild-type (WT) and knockout (KO) extensor digitorum longus (EDL) muscle components of the instantaneous stress (σ_{i_Ramp}), static stress (σ_{s_Relax}), dynamic stress (σ_d), Young's modulus (E) and half relaxation time ($t_{1/2}$) valuesinstantaneous stress (σ_{i_Ramp}), static stress (σ_s, σ_{s_Relax}), dynamic stress (σ_d), Young's modulus (E) and half relaxation time ($t_{1/2}$) values (mean ± sem) obtained with the ramp and relaxation tests. ** : $p < 0.01$ (Mann-Whitney's test).

	σ_{i_Ramp}	E	σ_{s_Relax}	σ_d	$t_{1/2}$
Macroscopic scale (WT vs KO)	0.328	0.328	0.248	0.328	0.929
Microscopic scale (WT vs KO)	0.001	0.004	0.011	0.002	0.647

	σ_s
Submicron scale (WT vs KO)	0.622